PNAS RESEARCH ARTICLE | IMMUNOLOGY AND INFLAMMATION

Redefining the human corneal immune compartment using dynamic intravital imaging

Laura E. Downie[a,1,2], Xinyuan Zhang[a], Mengliang Wu[a], Senuri Karunaratne[a], Joon Keit Loi[b], Kirthana Senthil[a,b], Sana Arshad[c], Kirstie Bertram[c], Anthony L. Cunningham[c], Nicole Carnt[c,d,e], Scott N. Mueller[b,1,2], and Holly R. Chinnery[a,1,2]

Edited by Michael Dustin, University of Oxford, Oxford, United Kingdom; received October 19, 2022; accepted June 13, 2023

The healthy human cornea is a uniquely transparent sensory tissue where immune responses are tightly controlled to preserve vision. The cornea contains immune cells that are widely presumed to be intraepithelial dendritic cells (DCs). Corneal immune cells have diverse cellular morphologies and morphological alterations are used as a marker of inflammation and injury. Based on our imaging of corneal T cells in mice, we hypothesized that many human corneal immune cells commonly defined as DCs are intraepithelial lymphocytes (IELs). To investigate this, we developed functional in vivo confocal microscopy (Fun-IVCM) to investigate cell dynamics in the human corneal epithelium and stroma. We show that many immune cells resident in the healthy human cornea are T cells. These corneal IELs are characterized by rapid, persistent motility and interact with corneal DCs and sensory nerves. Imaging deeper into the corneal stroma, we show that crawling macrophages and rare motile T cells patrol the tissue. Furthermore, we identify altered immune cell behaviors in response to short-term contact lens wear (acute inflammatory stimulus), as well as in individuals with allergy (chronic inflammatory stimulus) that was modulated by therapeutic intervention. These findings redefine current understanding of immune cell subsets in the human cornea and reveal how resident corneal immune cells respond and adapt to chronic and acute stimuli.

eye | cornea | T cell | macrophage | confocal

Significance

The corneal immune compartment plays an important role in protecting the eye from disease. Visualization of corneal immune cells has clinical and diagnostic utility. Yet, knowledge of the breadth of immune cell types in the human cornea is lacking. By performing non-invasive time-lapse imaging of the cornea in healthy humans, we identify that intraepithelial lymphocytes make up a substantial portion of cells in the epithelium. To date, these T cells have been classified as dendritic cells using static imaging. Our live imaging approach redefines understanding of the human corneal cellular immune landscape. Dynamic analysis reveals how corneal immune cells behave in the steady state and respond to acute and chronic proinflammatory stimuli, enabling rapid evaluation of immune responses in situ.

The cornea is an avascular, highly innervated sensory tissue. Together with a lack of blood or lymphatic vessels, the success of corneal transplant survival is regarded to derive from its status as an "immune-privileged" site (1) that limits inflammatory responses that can cause tissue opacity and impair vision. Based largely on findings in specific pathogen–free mice (2–4), the currently accepted paradigm is that the steady-state cornea has a solely innate immune cell profile. In these mouse corneas, dendritic cells (DCs) reside in the epithelium (2). As antigen-presenting cells, DCs are strategically located in the corneal surface layers (5, 6), ready to endocytose antigen, mature, and migrate to lymph nodes to elicit adaptive immune responses (7). The mouse corneal stroma is recognized to house mostly macrophages and some DCs (8–10).

The transparency and accessibility of the cornea afford non-invasive imaging of immune cells in living humans without fluorescent labeling, using commercially available in vivo confocal microscopy (IVCM) systems. Laser-scanning IVCM has a lateral resolution of ~1 μm and axial resolution of ~4 μm and delivers ~800-fold tissue magnification (11). Unlike conventional microscopes that diffusely illuminate a tissue sample, IVCM focuses light to a specific tissue depth, improving image resolution and contrast. Since the first description of confocal imaging to study the human eye ~30 y ago (12), IVCM has evolved as one of the major tools for examining the corneal microstructure in clinical and research settings.

Static IVCM image analysis is the current mainstay for studying human corneal immune cells (13). This approach involves analyzing cell density and morphology and has been largely limited to the epithelium. Hundreds of published papers have interpreted IVCM findings with a view that only DCs exist in the human corneal epithelium, as described in mice in the steady state (14). Based on this assumption, two main morphological subtypes of "presumed DCs" have been defined: "mature DCs" (>25 μm with long dendrites) and "immature DCs" (≤25 μm with shorter, less well-defined dendrites) (15). However, key limitations of static IVCM are the inability to analyze cell behaviors or to reliably disambiguate immune cells in the corneal stroma from the cell nuclei of fixed keratocytes.

Our team has pioneered a technique we term functional-IVCM (Fun-IVCM) to dynamically track immune cells over the corneal tissue depth in living human eyes, as a model tissue innervated by the peripheral nervous system. High-resolution volume scans of the cornea are sequentially acquired, and en face images are registered to fixed anatomical

Competing interest statement: L.E.D., X.Z., S.N.M., and H.R.C. are inventors on a patent relating to the imaging method described in this paper. National Health and Medical Research Council (NHMRC), APP1126540, funded the mouse experiments in this paper. There was no specific funding for the other aspects of this work.

This article is a PNAS Direct Submission.

[1]L.E.D., S.N.M., and H.R.C. contributed equally to this work.

[2]To whom correspondence may be addressed. Email: ldownie@unimelb.edu.au, smue@unimelb.edu.au, or holly.chinnery@unimelb.edu.au.

This article contains supporting information online at https://www.pnas.org/lookup/suppl/doi:10.1073/pnas.2217795120/-/DCSupplemental.

Published July 24, 2023.

features to generate time-lapsed videos. Fun-IVCM achieves unparalleled dimensionality to human in vivo immune cell analysis, with label-free longitudinal evaluation of cell density, morphology, and dynamics through the tissue depth. Images can be acquired at different tissue eccentricities to assess for regional effects.

In this study, we combine Fun-IVCM with multi-parameter flow cytometry and immunohistochemistry of human donor tissue to redefine the current understanding of the human corneal immune compartment. We define the dynamic behaviors of distinct morphological immune cell subsets and identify intraepithelial lymphocytes (IELs) in the steady-state human corneal epithelium that, to date, have been misclassified as DCs using static IVCM imaging. We provide in vivo descriptions of corneal epithelial DC and T cell surveillance behaviors, stromal immune cell dynamics, as well as immune cell-to-cell and neuroimmune interactions in a physiologically intact human tissue. Moreover, we show Fun-IVCM to be a unique and powerful tool for evaluating behavioral changes in corneal immune cells under non-homeostatic conditions, modeled by chronic immune activation due to seasonal allergy (16) and an acute pro-inflammatory stimulus induced by contact lens (CL) wear (17).

Results

Three Distinct Immune Cell Subsets Are Identified in the Healthy Human Cornea. To study the in vivo morphological and dynamic characteristics of human corneal immune cells, we performed Fun-IVCM (Fig. 1 *A* and *B*) in healthy adults (n = 16; age: mean ± SD, 29.7 ± 5.6 y [range: 22 to 39 y]; female/male ratio: 6/10). IVCM volume scans spanning the epithelium to mid-stroma (~100-μm depth) were captured at the inferonasal paracentral cornea (corneal whorl), every 4 to 7 min for 20 to 40 min. Images at each of the epithelial subbasal nerve plexus and anterior stroma were registered and reconstructed into time-lapsed videos to track individual immune cells (Fig. 1*C*).

We compared in vivo analyses of cell morphology and dynamic behavior in human corneas to features of corneal immune cells in transgenic fluorescent reporter mice. Based on dynamic behaviors and morphology, we identified three distinct corneal immune cell subsets in all human participants, namely T cells (Fig. 2 *A*, *i*) and DCs (Fig. 2 *A*, *ii*) in the epithelium, and macrophages (Fig. 2 *A*, *iii*) in the stroma. The density and morphological parameters of each immune cell subset, determined using Fun-IVCM, are summarized in *SI Appendix*, Table S1 and Fig. S1. The epithelial T cell subset comprised small, elongated, motile cells that patrolled the basal epithelium of the tissue (Fig. 2 *A*, *i*, Movie S1, and *SI Appendix*, Fig. S2). While these cells are referred to as immature DCs based on static IVCM imaging (15), their shape and behavior mirrored that of tissue-resident memory T cells (T_{RM} cells) characterized using intravital 2-photon microscopy in the cornea of live mice after ocular herpes simplex virus (HSV)-1 infection (18) (Fig. 2 *B*, *i* and Movie S2).

The second major cell subset identified in the human corneal epithelium comprised larger cells with a dendriform shape and obvious dendrites (Fig. 2 *A*, *ii*). The number of dendritic tips ranged from three to nine per cell (mean ± SD: 5.0 ± 1.8 tips/cell). Cells with this morphology are routinely termed "mature DCs" in humans based on their shape using static IVCM (15), rather than their activation state specifically. We newly describe the dynamics of these cells in the living human eye; they showed

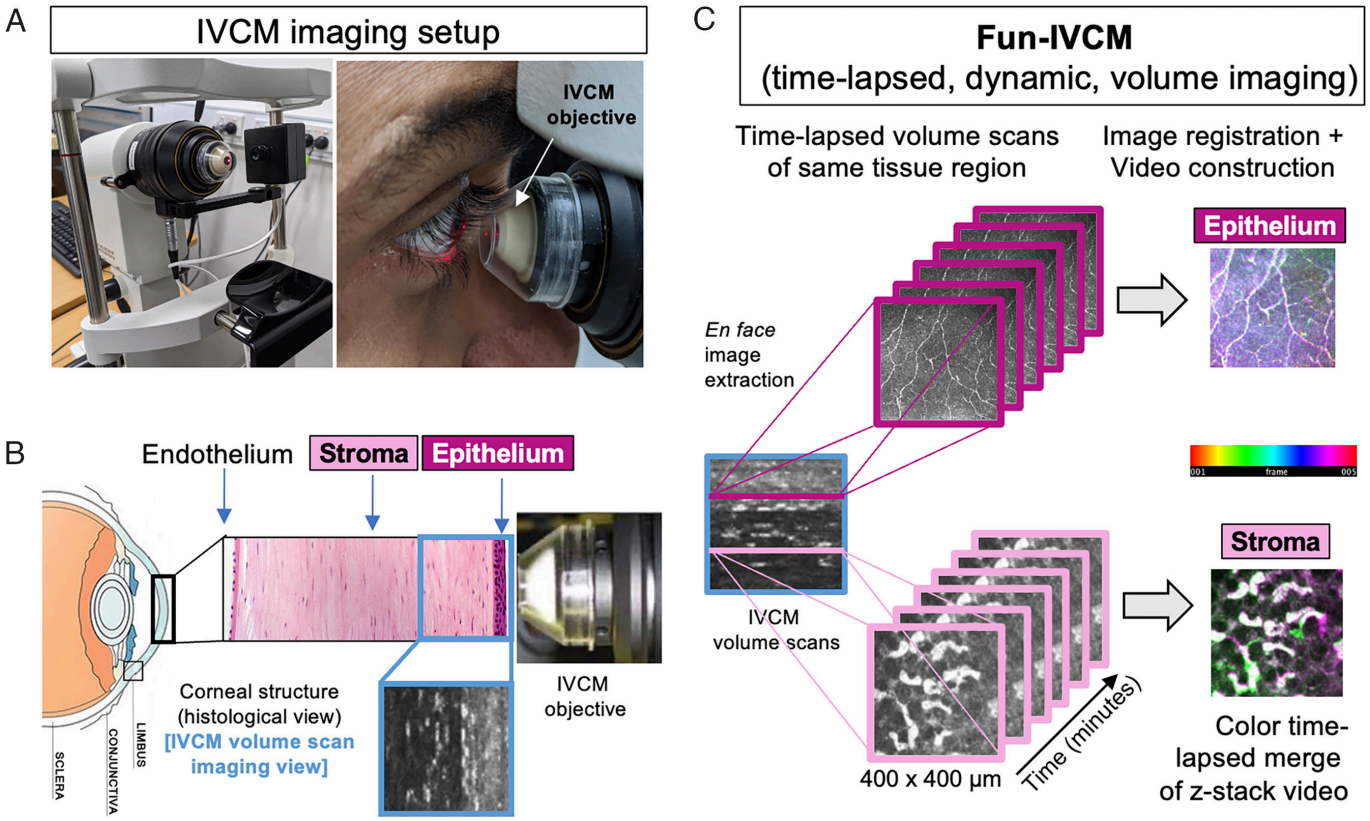

Fig. 1. Overview of the Fun-IVCM method. (*A*) Laser-scanning, IVCM setup with the Heidelberg HRT-3 with the Rostock Corneal Module, to acquire images of the human cornea (*B*), shown diagrammatically in histological cross-section [not to scale]. (*C*) The Functional IVCM (Fun-IVCM) method involves sequentially capturing high-resolution en face volume (z-stack) images [400(*x*) × 400(*y*) × 100(*z*) μm], spanning the basal layer of the corneal epithelium to the mid-stroma. Repeat volume scans of the same region are acquired every 4 to 7 min for a total of 25 to 40 min. En face images at the same tissue plane are extracted from the volume scans, registered to stationary landmarks, and time-lapsed videos are reconstructed at both the level of the corneal epithelium and anterior stroma.

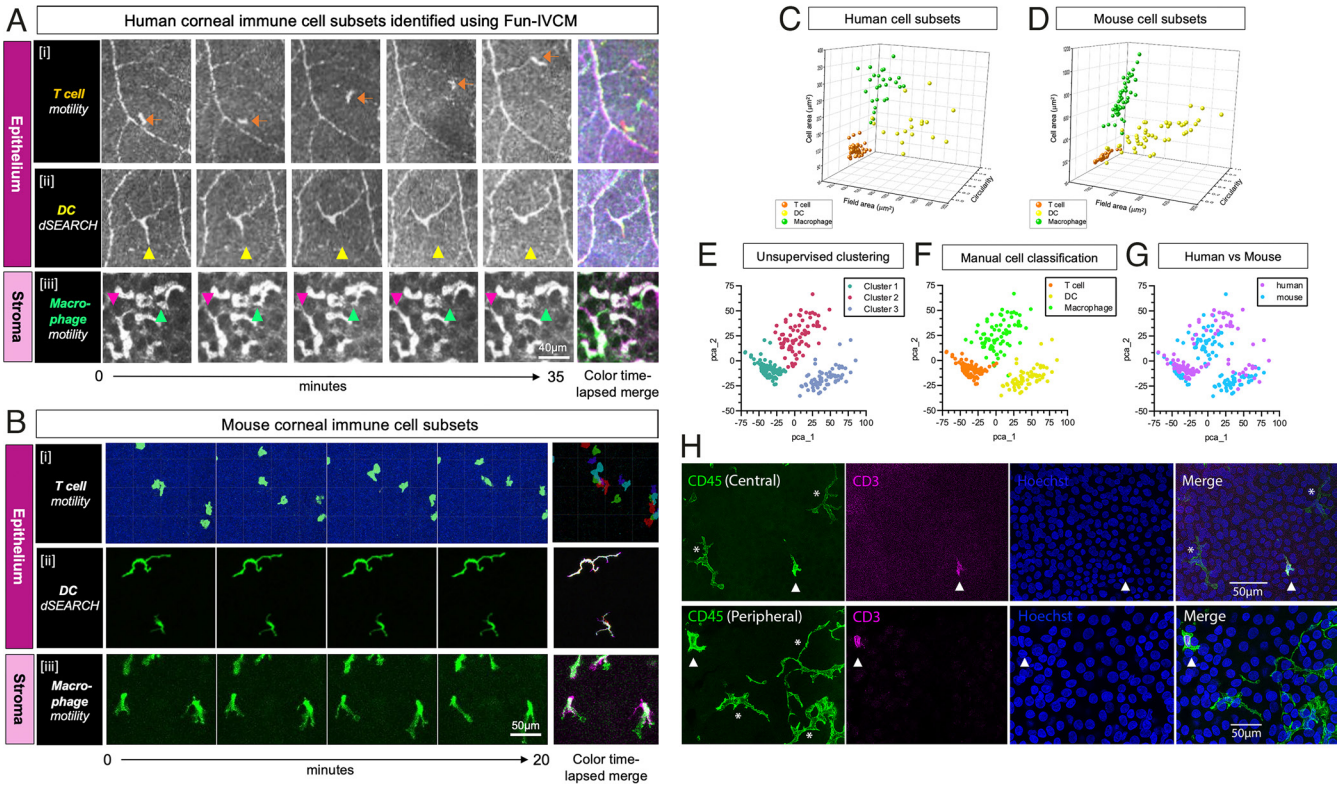

Fig. 2. Immune cell subsets defined using Fun-IVCM in healthy human corneas are comparable to phenotyped mouse corneal immune cell subtypes. (*A*) Sequential time-lapsed images acquired over 35 min, and a color time-lapsed merge, captured using Fun-IVCM to reveal the dynamic behaviors of putative [*i*] T cells (orange arrow tracks a single cell) that are motile in the human corneal epithelium; [*ii*] DCs showing dSEARCH behaviors (the yellow triangle is stationary and highlights active dendrite retraction); and [*iii*] macrophages in the corneal stroma that crawl between keratocyte nuclei (pink and green arrows highlight the alterations to cell position over the capture period). The scale bar applies to all images. (*B*) Sequential time-lapsed images and color time-lapsed merges for each of: [*i*] GFP+ T cells in the corneal epithelium of a mouse with ocular HSV infection, imaged in vivo using intravital 2-photon microscopy; [*ii*] CD11c-eYFP+ mouse corneal epithelial DCs, imaged ex vivo; [*iii*] CX3CR1-GFP+ corneal macrophages. The scale bar applies to all images. (*C*) 3D scatterplot showing the field area (μm) x circularity x solidity parameters for the three immune cell subsets in healthy human corneas, quantified from Fun-IVCM images. (*D*) An equivalent 3D scatterplot to (*C*), for phenotyped mouse corneal immune cells. Cell parameters were quantified from wholemount immunofluorescent images and show cell morphological characteristics that parallel the human corneal cell subsets imaged using Fun-IVCM. (*E*) 2D pca plot showing three clusters of immune cells determined by unsupervised clustering of normalized and pooled human and mouse imaging data using PhenoGraph. (*F*) Subtypes of immune cells determined manually from imaging data projected onto the pca scatter plot. (*G*) Human and mouse corneal immune cells projected onto the pca plot, revealing clustering by cell type not by species. (*H*) Wholemount immunostaining of human donor tissue showing $CD45^+$ $CD3^+$ T cells (triangles) and $CD45^+$ $CD3^-$ dendriform cells (asterisks) present in the basal epithelium of the healthy central and peripheral corneal epithelium.

minimal lateral migration and repeated, active extension and retraction of their dendrites (Movie S3). Their shape (Fig. 2 *A*, *ii*) and behavior were consistent with the probing behavior of DCs in the healthy corneal epithelium of CD11c-eYFP mice (Movie S4 and Fig. 2 *B*, *ii*) and DCs in other tissues (19).

In the human corneal stroma, we observed amoeboid-shaped cells with a veiling motion that appeared to use membrane extensions to squeeze past presumed keratocyte nuclei (Fig. 2 *A*, *iii* and Movie S5). These dynamic cells were distinguished from stationary stromal landmarks using Fun-IVCM; static IVCM does not allow their identification. The cells' morphology (Fig. 2 *A*, *iii*) and behavior appeared analogous to corneal macrophages (Fig. 2 *B*, *iii*) imaged in vivo in CX3CR1-GFP mice (Movie S6). On rare occasions, small, highly motile cells were seen in the stroma that we surmised were T cells, corresponding to fast-moving amoeboid cells in the corneal stroma in mice (18). The morphological similarities between these three major immune cell subsets in both human (Fig. 2*C*) and mouse (Fig. 2*D*) corneas are presented as a 3D scatterplot. To verify whether unsupervised clustering analysis could identify the three immune cell types from imaging data parameters, normalized data from human and mouse cornea were pooled together. Unbiased cluster analysis was performed using the morphological parameters, including cell area, field area, and circularity. Three distinct immune cell clusters were identified, representing T cells, DCs, and macrophages (Fig. 2 *E*–*G*). Notably, the clustering results demonstrated a high level of concordance with the manual image classification (Fig. 2*F*), and both human and mouse corneal immune cells were clustered equivalently (Fig. 2*G*), suggesting that identification of corneal immune cell types by imaging parameters is conserved and comparable across species.

While the presence of DCs in the human corneal epithelium is widely accepted, there is little evidence for the existence of T cells in the steady-state cornea. Using wholemount immunofluorescence staining of human donor tissue, $CD45^+$ $CD3^-$ dendriform cells, exhibiting long slender processes, were identified in the corneal epithelium alongside small $CD45^+$ $CD3^+$ T cells (Fig. 2*H*), which displayed a morphology similar to the motile cells observed using Fun-IVCM (Fig. 2 *A*, *i*). As further evidence of T cells in the healthy human cornea, flow cytometry on dissociated human corneal tissues confirmed the presence of $CD3^+$ T cells, $CD1c^+$, and $Langerin^+$ DCs (20) and macrophages [autofluorescent positive, which have been shown to be resident macrophages (21), and nonautofluorescent monocyte-derived macrophages (22, 23)] in both the epithelium and stroma (*SI Appendix*, Fig. S3). We also confirmed that morphologically comparable immune cells exist in the basal epithelium of HSV-infected CX3CR1-deficient mouse corneas, using static IVCM (*SI Appendix*, Fig. S4); CD3 immunostaining of these mouse corneas ex vivo, to confirm their T cell identity, shows

morphological homology between the stained T_{RM} cell population, and the immune cells seen using IVCM. These cells are unlikely to be DCs as CX3CR1-deficient mice lack corneal epithelial DCs (24). Together, these findings are consistent with the conclusion that the small, motile immune cells that lack visible dendrites in the healthy human corneal epithelium are T cells rather than "immature DCs".

Additionally, stationary, hyper-reflective round/oval-shaped bodies, termed "globular cells" in the current literature (25), were observed in the corneal epithelial whorl (Fig. 3*A*).

The Healthy Corneal Epithelium Is Patrolled by IELs, Which Show Enhanced Motility and Differential Changes in Density with Chronic vs. Acute Inflammatory Stimuli. We next used Fun-IVCM to provide insight into the effect(s) of chronic immune-mediated disease (ocular allergy, with and without immunomodulatory treatment) and an acute ocular surface inflammatory stimulus (short-term CL wear) on corneal immune cell subsets. This study involved three age- and sex-matched participant groups: healthy controls (n = 16); individuals with seasonal ocular allergy without concomitant medical management (n = 10, untreated allergy); and individuals with seasonal ocular allergy who had recently received immunomodulatory treatments (n = 4 treated allergy; comprising n = 2 nasal corticosteroids and n = 2 allergen immunotherapy). Participant demographics are summarized in *SI Appendix*, Table S2.

The cell density and behavioral dynamics of epithelial T cells were quantified in time-lapsed videos (Fig. 3*A*) generated for each participant. In total, 130 T cells were analyzed (healthy controls: n = 65; untreated allergy: n = 41; treated allergy: n = 24, comprising 12 cells from individuals treated with systemic immunotherapy and 12 cells from individuals treated with corticosteroids). These cells were similarly frequent in the central and paracentral cornea in all participant groups (Fig. 3*B*), indicating an inability to differentiate between healthy and disease states based on the traditional static IVCM parameter of cell density. There was a positive correlation between cell density across corneal regions within individuals (Fig. 3*C*, $R^2 = 0.43$, $P < 0.0001$). In corneas with untreated seasonal allergy, epithelial T cells had a higher mean instantaneous speed (Fig. 3*D*) and lower arrest coefficient (Fig. 3*E*) than healthy controls or those with treated ocular allergy. Within the treated allergy group, there was a tendency for a greater degree of normalization of T cell instantaneous speed with the use of immunotherapy compared with corticosteroid treatment (Fig. 3*D*). Other motility parameters, including cell displacement speed, meandering index, displacement ratio, linearity of forward progression, and mean directional change, were similar between groups ($P > 0.05$ for all comparisons).

The effect of an acute, provocative stimulus, in the form of a CL, was evaluated in a subpopulation of healthy adults. Participants underwent baseline (pre-CL) and repeat Fun-IVCM imaging of the same corneal region after 3 h of CL wear (post-CL). Post-CL, the density of epithelial T cells was half that of pre-CL levels (Fig. 3*F*; mean ± SD, pre-CL: 22.7 ± 11.5 vs. post-CL: 10.2 ± 7.4 cells/mm^2, $P = 0.047$). The remaining cells had a higher mean instantaneous speed (Fig. 3*G*), lower arrest coefficient (Fig. 3*H*), higher displacement speed (Fig. 3*I*), higher meandering index (Fig. 3*J*), and higher linearity of forward progression (Fig. 3*K*). Individual cell tracks over a 20-min period, from the pre-CL (Fig. 3*L*) and post-CL (Fig. 3*M*) time points, depict the extent of the inter-condition differences in cell motility.

Fun-IVCM identified IELs patrolling the healthy human corneal epithelium. Individuals with untreated ocular allergy had a similar number of T cells, but they had enhanced motility; these altered cell behaviors were normalized in individuals with allergy treated using immunomodulatory agents. An acute inflammatory stimulus induced more pronounced immune cell changes, with reduced T cell density in the paracentral corneal epithelium that suggests active cell migration, and the remaining cells showed vastly enhanced tissue surveillance.

Dynamic Probing Behavior of Corneal Epithelial DCs under Homeostatic Conditions Is Suppressed by Ocular Surface Inflammation. In healthy corneas, putative DC density was similar in the central and paracentral regions; eyes with seasonal allergy had fewer cells in the paracentral cornea (Fig. 4*A*). Dendrite dynamics were quantified using the dendrite surveillance extension and retraction cycling habitude (dSEARCH) (19). dSEARCH was evident in all 20 imaged DCs, to varying degrees. We quantified the dSEARCH index per minute (normalized dSEARCH index), representing the cumulative distances of dendrite extension and retraction observed for a given DC per unit of time. Cells with more dendritic complexity generally had a higher normalized dSEARCH index (Fig. 4*B*, $R^2 = 0.41$, $P = 0.0022$), indicating that cells with more dendrites facilitated greater local tissue surveillance. Inter-group comparisons were limited by very few corneal DCs in eyes with seasonal allergy; the two cells captured showed low dynamic activity (Fig. 4*C*).

With respect to an acute, CL-induced inflammatory stimulus (26, 27), at the participant level, DC density did not change from baseline (Fig. 4*D*). For cell-level analyses, the same DCs (n = 32) were analyzed using repeated measures by matching cell locations to nerve landmarks (Fig. 4*E*). Post-CL wear, DC dendritic complexity was reduced (mean ± SD, pre-CL: 5.0 ± 2.0 vs. post-CL: 4.2 ± 1.5 tips/cell, $P = 0.042$). Of the 32 matched DCs, most (75%, n = 24) maintained their pre-CL dendritic orientation following CL wear, although 25% (n = 8) showed shifts ≥90 degrees (Fig. 4 *E* and *F*). Representative color time-lapsed merges for pre- vs. post-CL wear conditions show reduced dSEARCH behavior after CL wear (Fig. 4 *E* and *F*). The normalized average dSEARCH index was overall lower post-CL wear (Fig. 4*G*, mean ± SD, pre-CL: 3.29 ± 2.05 vs. post-CL: 2.52 ± 1.41 dSEARCH index/minute, $P = 0.0052$).

In summary, Fun-IVCM imaging enabled quantification of DC dendrite surveillance in healthy human corneas and identified a relative suppression of this constitutive behavior under non-homeostatic, pro-inflammatory conditions.

Fun-IVCM Reveals Dynamic Immune Cell-To-Cell and Neuroimmune Interactions in the Human Cornea. We captured in vivo dynamic immune cell-to-cell and neuroimmune interactions in the corneal epithelium. Of 65 IELs tracked in healthy corneas, 22 (34%) appeared to interact with sensory nerves. The most frequent type of cell-to-nerve interaction was an IEL crossing a nerve (n = 17; Fig. 5*A*, green triangle). Less frequently (n = 5), IELs appeared to "kiss" nerves; a cell would touch a nerve axon and rebound toward the area it approached from (Fig. 5*A*, blue triangle). The average speed of the cell on its initial approach was less than its speed after nerve interaction (Fig. 5*B*; mean ± SD, before: 1.25 ± 0.83 vs. after: 1.92 ± 0.61 μm/min, $P = 0.043$, Movie S7), suggesting potential modification to IEL behavior from the nerve interaction. T cell-to-T cell interactions were infrequent; a representative example is provided in Fig. 5*C*.

T cells also transiently contacted DC dendrites (Fig. 5 *D*–*F* and Movie S8). A similar interaction, with a $CD11c^+$ cell contacting a $CD3^+$ T cell, is shown in the mouse corneal epithelium using wholemount ex vivo immunohistochemistry (Fig. 5*G*). Of the 18 DCs quantified from control eyes, six cells (33%) dynamically extended their dendrites to interact with sensory nerves (Fig. 5 *F* and *G*).

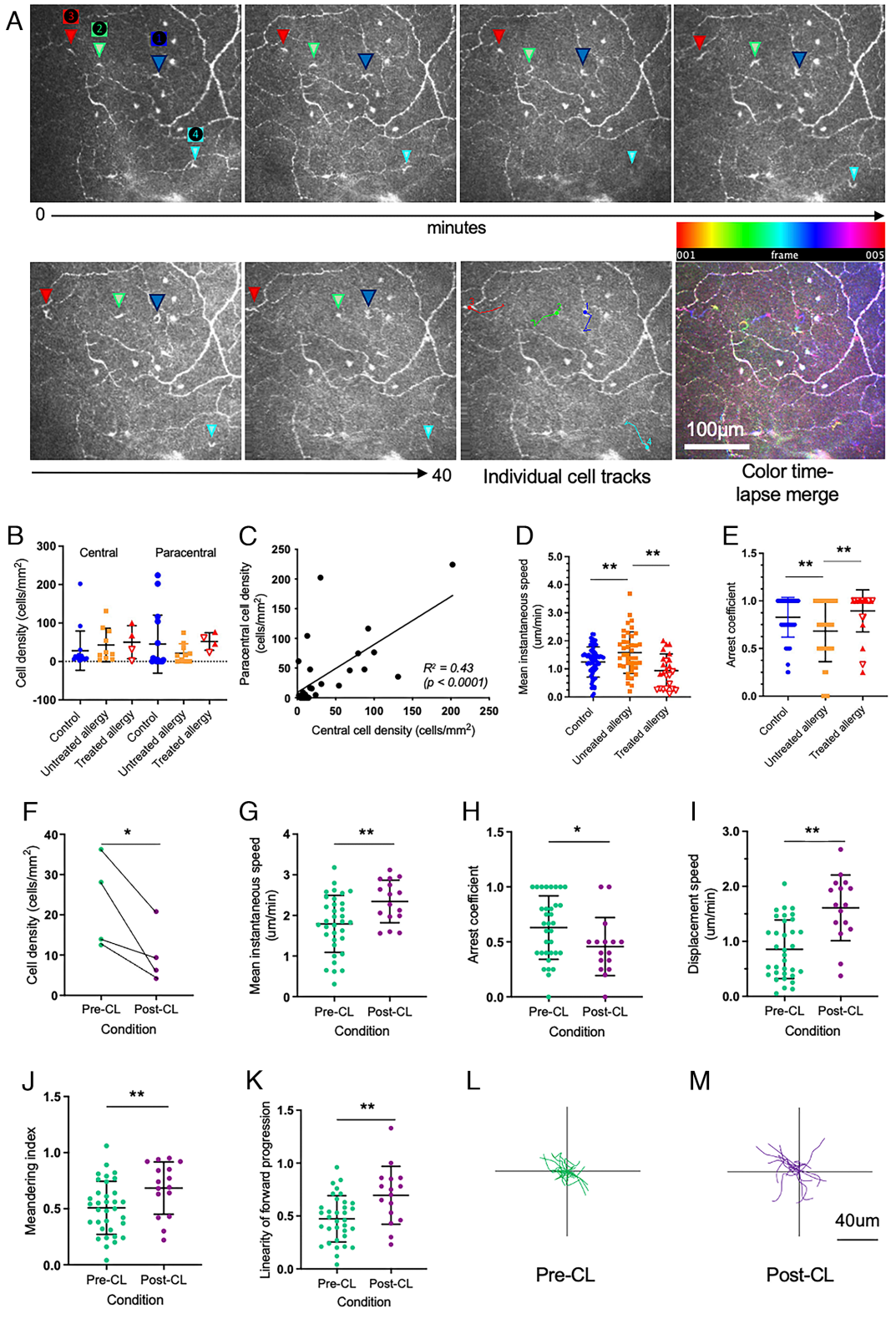

Fig. 3. IELs dynamically patrol the corneal epithelium and are responsive to inflammatory stimuli. (*A*) Sequential time-lapsed images acquired over 40 min, with four individual cells noted (triangles labeled 1 to 4). Individual cell tracks and a color time-lapsed merge are also shown. The scale bar applies to all images. (*B*) Cell densities were similar in the central and paracentral cornea, and in control (n = 16 people), untreated allergy (n = 10 people), and treated allergy (n = 4 people; open triangles represent individuals treated with immunotherapy [n = 2], and closed triangles represent individuals treated with corticosteroids [n = 2]) eyes ($P > 0.05$ for all comparisons). (*C*) Cell density in the central and paracentral corneal regions was moderately correlated ($R^2 = 0.43$, $P < 0.0001$). (*D*) Mean instantaneous cell speed was significantly higher in individuals with untreated allergy (n = 41 cells), relative to speeds evident in both healthy control (n = 65 cells) and treated allergy (n = 24 cells) eyes. (*E*) The mean arrest coefficient was significantly lower in individuals with untreated allergy, relative to both healthy control and treated allergy eyes. (*F*) After short-term CL wear, there were significantly fewer cells in the paracentral corneal epithelium relative to pre-CL levels. Post-CL wear, cells showed a faster mean instantaneous speed (*G*), lower arrest coefficient (*H*), higher displacement speed (*I*), higher meandering index (*J*), and higher linearity of forward progression (*K*). Individual cell tracks prior to CL wear (pre-CL) (*L*), and after 3 h of CL wear (post-CL) (*M*), after normalization of starting positions to the origin. Data are plotted as mean ± SD. *$P < 0.05$; **$P < 0.01$.

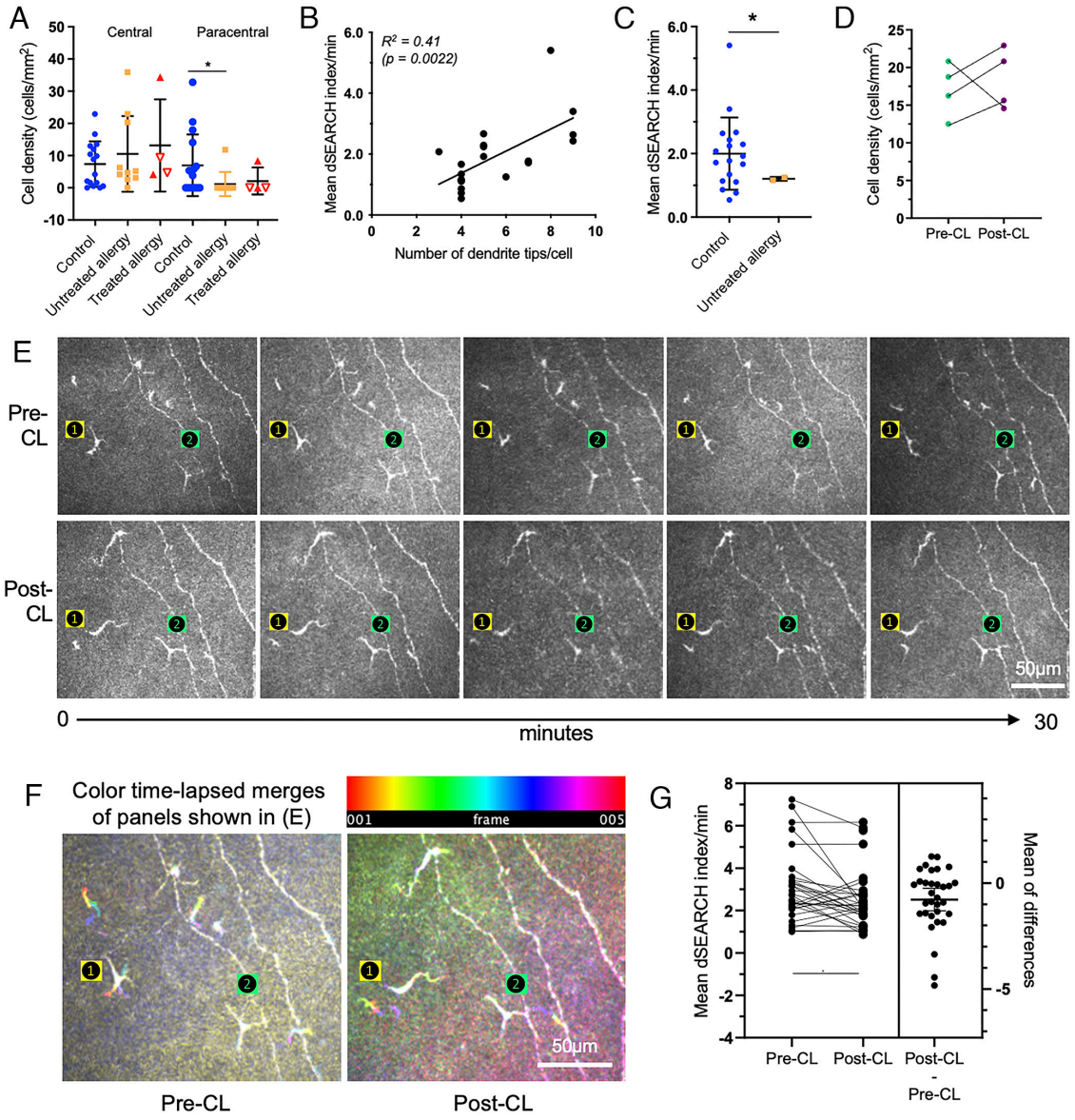

Fig. 4. DCs use their dendrites to dynamically survey the human corneal epithelium and show muted responses when exposed to inflammatory stimuli. (*A*) Cell densities were similar across participant groups (healthy, n = 16; untreated allergy, n = 10; treated allergy, n = 4 comprising individuals treated with immunotherapy [open triangles, n = 2] and individuals treated with corticosteroids [closed triangles, n = 2]) in the central cornea ($P > 0.05$). In individuals with untreated allergy, there were fewer DCs in the paracentral cornea relative to healthy controls ($P < 0.05$). (*B*) DCs with more dendritic complexity (tips/cell) generally had a higher mean dSEARCH index per minute ($R^2 = 0.41$, $P = 0.0022$). (*C*) Mean normalized dSEARCH was lower in cells in individuals with untreated allergy (n = 2 cells), relative to healthy controls (n = 18 cells). (*D*) Cell numbers were unchanged after 3 h of CL wear. (*E*) Sequential time-lapsed images acquired over 30 min, with two individual cells noted (labeled 1 and 2), at the pre-CL (*Upper row*) and post-CL (*Lower row*) time points. Cell 1 underwent a shift in its dendritic orientation post-CL wear, whereas the overall dendritic conformation of cell 2 was unchanged. The scale bar applies to all images. (*F*) Color time-lapsed merges of the *Upper* and *Lower* panels shown in (*E*), respectively. The pre-CL merge shows more obvious dSEARCH activity (Cell 1 > 2), which was reduced in the post-CL merge. Data are plotted as mean ± SD. The scale bar applies to both images. (*G*) Data for matched cells (n = 32), analyzed pre-CL vs. post-CL wear, show that the normalized average dSEARCH index was lower post-CL wear. *$P < 0.05$.

Dynamic, Macrophage-Like Cells in the Corneal Stroma Are Morphologically Different in Individuals with Allergy and Altered by CL Wear. Time-lapsed imaging of the anterior stroma revealed the presence of motile amoeboid-shaped cells, that closely resembled the dynamic crawling and lamellipodial features of macrophages observed in the corneal stroma of CX3CR1-GFP mice (Fig. 2 *B*, *iii*). These large, hyperreflective cells (Fig. 6*A*, orange arrowheads) were in the anterior-most layers of the stroma, adjacent to stationary keratocytes, which are resident fibroblast-type cells of the cornea (pink arrows). Compilation of cell area masks over the imaging period (Fig. 6*A*) showed overt differences in the morphology of the motile cell population (cyan), compared to the stationary keratocytes (magenta). Quantitative analysis of the fluctuations in the area of individual cells over time (as measured by the coefficient of variation, Fig. 6*B*) demonstrated the greater extent of variability in cell morphology in the macrophage-like cells (14.8%, n = 20 cells) compared to the relatively homogenous keratocytes (5.6%, n = 21 cells, $P < 0.0001$).

In the healthy human corneal stroma (Fig. 6*C*), stationary keratocytes were the most abundant cell type (573.5 ± 51.9 cells/mm^2), followed by putative macrophages (85.9 ± 18 cells/mm^2). In less than half of participants, low numbers of highly motile T cells (classified based on their migratory speeds and morphological features that closely resembled epithelial T cells) were observed (10.0 ± 5.6 cells/mm^2; Fig. 6*C*). In individuals with treated and untreated allergy, the density of stromal macrophages was similar to healthy

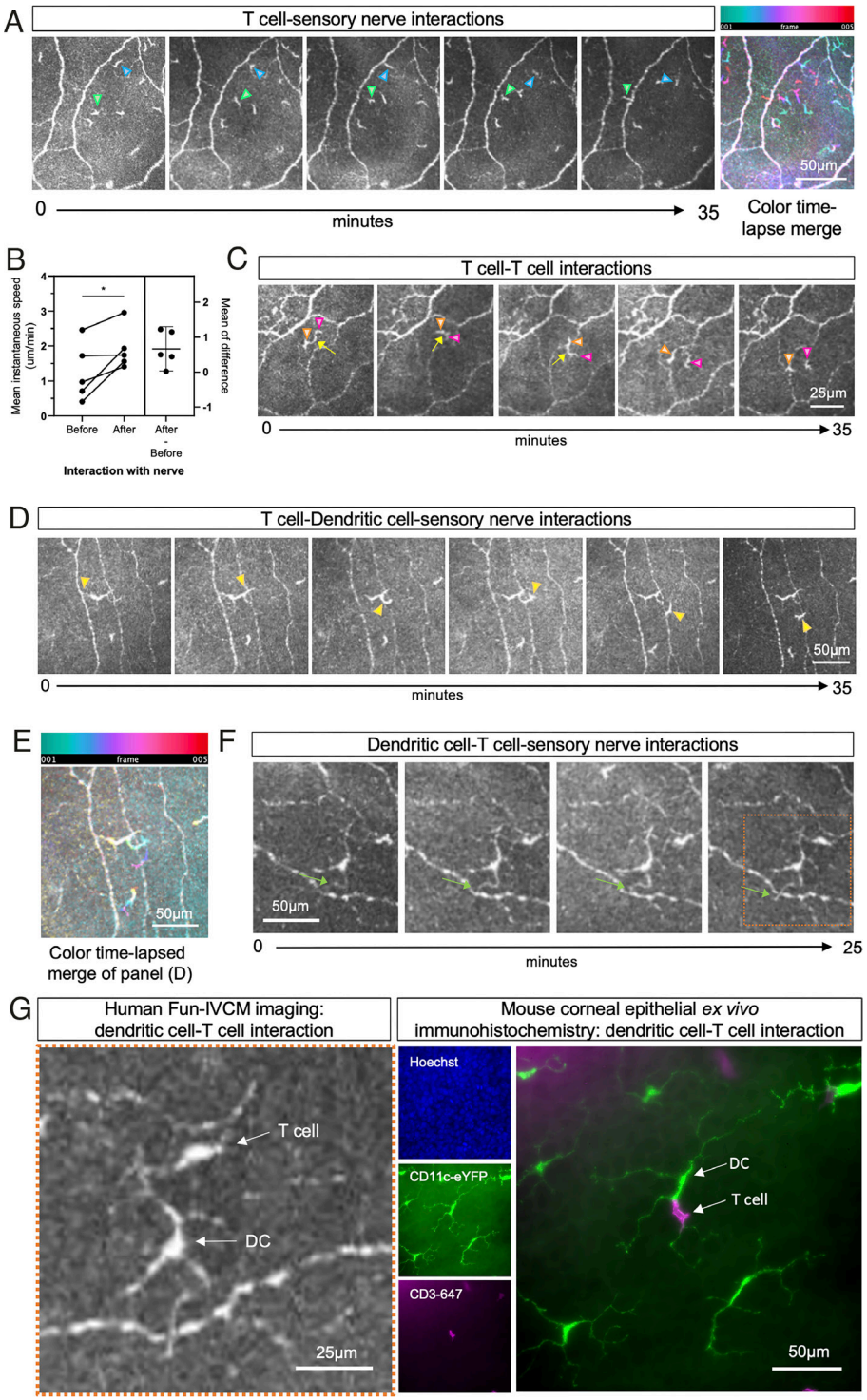

Fig. 5. Fun-IVCM captures dynamic immune cell-to-cell interactions and neuroimmune interactions in the human cornea. (*A*) Sequential time-lapsed images of the corneal epithelium, acquired over 35 min, showing examples of a T cell crossing a sensory nerve axon (green triangle) and a separate cell "kissing" a nerve before rebounding back to its original location (blue arrow). A color time-lapsed merge highlights the cell motility dynamics. The scale bar applies to all images. (*B*) Plot of data for matched cells seen to "kiss" nerves (n = 5), showing the cells to have a higher mean instantaneous speed after their interaction with a nerve ("After") relative to approaching the nerve ("Before"). (*C*) Sequential time-lapsed images showing an example of two motile T cells (orange and pink triangles) that appear to maintain contact with each other for several minutes. The scale bar applies to all images. (*D*) Sequential time-lapsed images, and a corresponding color time-lapsed merge (*E*), showing dynamic interactions between a T cell, DC, and nerve axon. (*F*) Sequential time-lapsed images showing a DC dendrite dynamically moving across a nerve axon (green arrow). The scale bar applies to all images. (*G*) The left images show a magnified *Inset* (orange box) of the final image in panel (*F*), to highlight a DC–T cell interaction in the human cornea using Fun-IVCM. The right images show wholemount immunofluorescent images from a mouse corneal epithelium, stained for cell nuclei (Hoechst), DCs (CD11c-eYFP), and T cells ($CD3^+$); the DC–T cell interaction mirrors the appearance of the in vivo human corneal imaging shown in (*G*).

controls (control vs. untreated allergy, $P = 0.367$; control vs. treated allergy, $P = 0.066$; Fig. 6*D*). Macrophages in the allergy group had a smaller cell area (Fig. 6*E*; mean ± SD, 251 ± 71 μm^2) compared to healthy controls (cell area 312.1 ± 76 μm^2; $P = 0.0043$). Cells in the treated allergy group were larger than in both the healthy and allergy groups (cell area 376 ± 70 μm^2; perimeter 131 ± 19 μm;

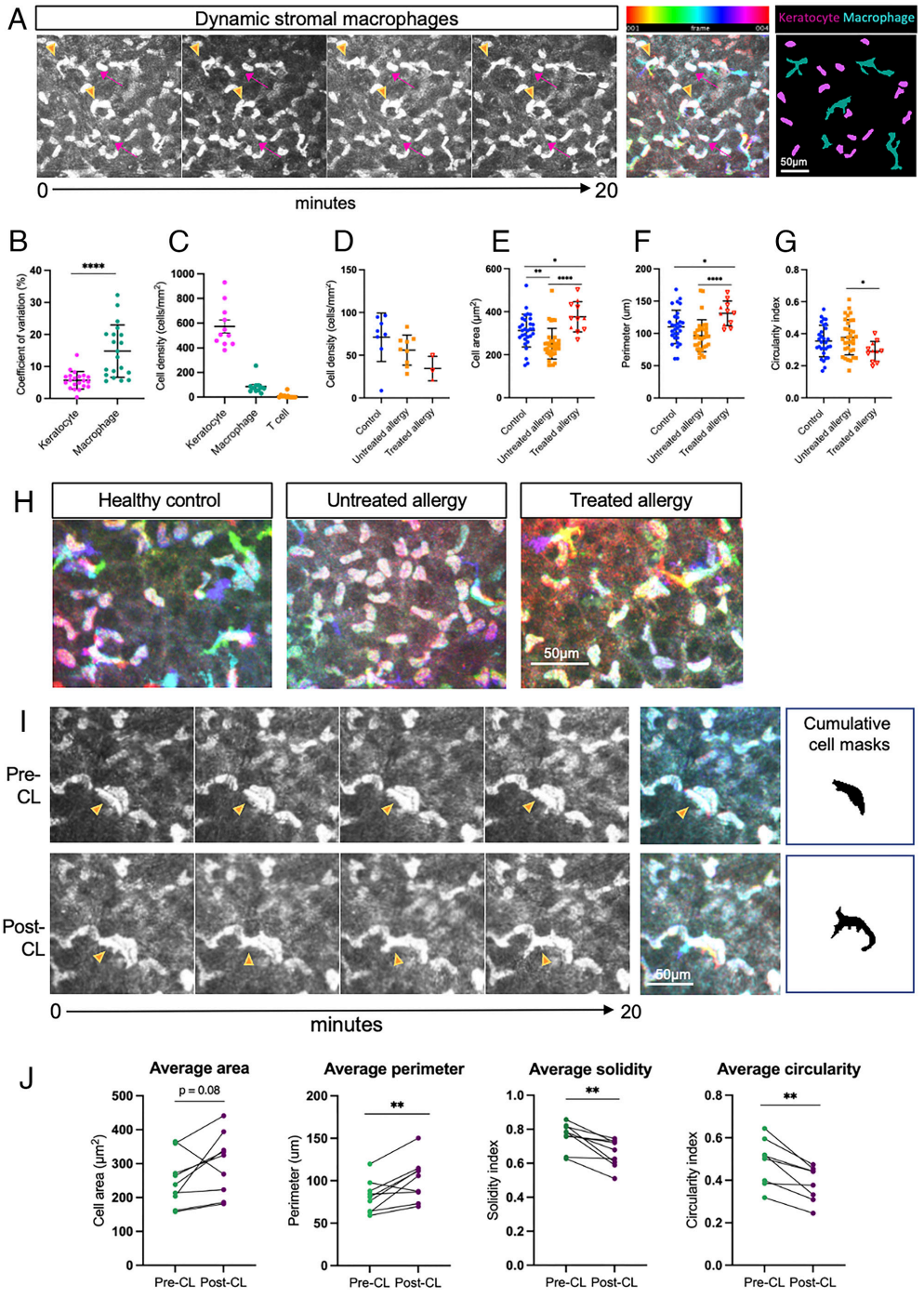

Fig. 6. Putative stromal macrophages are morphologically and behaviorally distinct from resident tissue keratocytes and are affected by allergy and acute stimulation elicited by CL wear. (*A*) Sequential time-lapsed images of the anterior stroma in a healthy control cornea over a 20-min period. Stationary keratocytes (pink arrows) and motile cells (orange arrowheads) demonstrate differential behaviors. A color-coded hyperstack shows cytoplasmic displacement in macrophages, and cumulative cell masks show small-shaped keratocytes (magenta) compared to ameboid-shaped macrophages (cyan). (*B*) The coefficient of variation of cell shape over time was higher in macrophages compared to keratocytes. (*C*) Keratocytes represent the major cell type in the anterior stroma, followed by macrophages and T cells. (*D*) There was a similar density of stromal macrophages in individuals with untreated and treated allergy compared to healthy controls. Per cell analysis plots of cell area (*E*), perimeter (*F*), and circularity (*G*) show differences in the morphology of stromal macrophages in control vs. treated and untreated allergy. (*H*) Representative time-lapse color-coded hyperstacks of stromal macrophages in healthy control, untreated allergy, and treated allergy individuals. (*I*) Time-lapse image sequence and corresponding color-coded hyperstacks and cumulative cell area masks of a stromal macrophage pre-CL (*Top row*) and post-CL (*Bottom row*). (*J*) Repeated measures comparisons of the area, perimeter, solidity, and circularity of the same stromal macrophages (n = 9) were quantified pre-CL and post-CL. Scale bars are as indicated. Data are plotted as mean ± SD. **P* < 0.05; ***P* < 0.01, ****P* < 0.001, *****P* < 0.0001.

Fig. 6*F*) and also had a lower circularity index (0.29 ± 0.07 [allergy-treated] vs. 0.35 ± 0.10 [control] vs. 0.38 ± 0.10 [allergy untreated]).

To examine whether an acute inflammatory stimulus altered stromal macrophage morphology, matched cells from the same corneal location were measured before (pre-CL) and 3 h after a CL was applied (post-CL) to the eye (Fig. 6*I*). Color-coded depth projections and cumulative cell masks depict the total area covered by a representative cell after 20 min of imaging and show a higher number of cellular protrusions at the post-CL time point (Fig. 6*I*). Quantitative repeated measures analyses were performed on a total of nine matched cells from four individuals (Fig. 6*J*). Compared

to baseline (pre-CL), stromal macrophages after CL wear tended to be larger (pre- vs. post-CL wear: cell area, $P = 0.085$; cell perimeter, $P = 0.009$) and had lower solidity ($P = 0.003$) and a reduced circularity index ($P = 0.001$).

Model of Steady-State Human Corneal Immunology. In contrast to the long-held view that the healthy human cornea only houses innate immune cells (Fig. 7 *A*, *i*) (28), we show the coexistence of innate (DC and macrophage) and adaptive (T cell) immune cells, including a putative population of T_{RM} cells that patrol the epithelium under homeostatic conditions (Fig. 7 *A*, *ii*). We demonstrate that chronic (Fig. 7 *B*, *i*) and acute (Fig. 7 *B*, *ii*) inflammatory stimuli induce differential effects on innate and adaptive immune cell subtypes, spanning the epithelial and stromal corneal layers.

Discussion

Insights provided by Fun-IVCM, married with our complementary in vivo and ex vivo analyses of immune cells in mice, and ex vivo analyses of donor healthy corneas redefine our understanding of human corneal cellular immunology. We identify three distinct immune cell subsets, distinguished by their shape and dynamics: i) IELs: small, motile cells whose shape and movement parallel T cells seen using intravital 2-photon imaging in mice after viral infection (18); ii) DCs: larger cells with obvious dendrites populating the epithelium that show minimal lateral migration (19, 29); and iii) macrophages: amoeboid and/or star-shaped cells in the stroma that appear to crawl between keratocytes (30). We show that the morphological and dynamic features of these corneal immune cell subsets, imaged in living humans in vivo, are congruent with ex vivo immunohistochemical staining of human donor tissues, and observations in fluorescent gene reporter mice, analyzed using in vivo and ex vivo approaches. Flow cytometry on healthy human donor corneas provides evidence for the presence of $CD3^+$ T cells in the epithelium and stroma and smaller percentages of DCs and macrophages.

The cornea is traditionally considered an "immune-privileged" site, due to its avascularity, tight surface barriers, and regulated immune cell surveillance (31). Current understanding of its immune cell landscape derives primarily from mouse studies, with presumed generalizability to humans. The steady-state cornea is generally accepted to house DCs in the epithelium and macrophages in the stroma (2–4, 8). Over the past 30 y, the >200 publications that have evaluated human corneal immune cells using static IVCM refer to immune cells in the epithelium as DCs or Langerhans cells. Our data challenge this dogma (28), revealing a previously unrecognized population of patrolling T cells. We recently reported that HSV-1 infection induces the formation of tissue-resident memory T (T_{RM}) cells in the mouse cornea; these cells are present at 30 d postinfection, being a time point well past the acute phase of infection, and closely match the morphology and dynamic behaviors of epithelial immune cells in normal human corneas (18). T cells were also observed to infiltrate the cornea in a mouse model of corneal allograft rejection (32). These CXCR6-GFP^+ T cells displayed dynamic cell morphologies that correlated with motility. The presence of high numbers of cells with equivalent morphology in the corneal epithelium in disease states characterized by infective processes [e.g., in long-COVID patients (33), during infectious keratitis (34), including from viral, bacterial, and fungal pathogens] also aligns with the notion that the cells enter the tissue in response to infection, as would be expected from adaptive immune cells. While none of the 30 participants in the current study had a known history of corneal infection, putative T cells were imaged in all individuals. Common and less severe ocular surface infections (e.g., viral conjunctivitis) or exposure to environmental antigens may be sufficient to induce corneal T_{RM} formation. T_{RM} phenotype cells exist in the human conjunctiva (35), and the IELs identified in our study could represent diverse populations of T cells, including conventional and unconventional T cells, such as γδ T cells. Further work is underway to define the phenotype and antigen specificity of corneal resident T cells and to examine how they are impacted by age and other stimuli.

We also observed dynamic corneal neuroimmune interactions in vivo. Neuroimmune cross talk is established in barrier surfaces such as the gut, skin, and airway (36), with growing evidence for similar interactions in the cornea (37–39). A limitation of prior human studies, using static imaging, is their inability to capture cell spatiotemporal dynamics (36). Using Fun-IVCM, we imaged dynamic DC–nerve interactions, with dendritic tips episodically interacting with nerve axons. These findings align with data showing the structural interdependence of epithelial DCs and sensory nerves in the mouse cornea (10), which has been linked to nerve function and repair (10, 40). We also noted "kissing" interactions between T cells and nerves that appeared to lead to increased cell motility postcontact. T cells can also interact with other cells that express antigens or chemokines (41), such as epithelial cells and keratocytes, which warrants investigation in the corneal epithelium and stroma, respectively. Capturing these interactions between the nervous and immune systems in the living human eye, using Fun-IVCM, provides opportunities to study the interface between nerves and immune cells in an intact peripheral sensory tissue, including how exogenous factors and disease may disrupt the perception, integration, and responsiveness of cell subtypes to different challenges.

Distinct changes to corneal immune cell dynamics were observed under non-homeostatic conditions. We evaluated eyes with symptomatic seasonal allergy (as a model of chronic immune activation) (16) and before and after CL exposure [as an acute inflammatory stimulus (42)]. We found differential effects on the density, morphology, and behavior of immune cell subsets. Corneal T cells in people with symptomatic ocular allergy had higher motility and a lower arrest coefficient, indicating heightened tissue surveillance (43). Although the mechanism through which T cells adapt their motility is unclear (44), tissue inflammation can increase T cell speeds in vivo (45). This increased adaptive corneal immune cell activity in allergy was accompanied by a relative suppression of innate immune cells, with fewer epithelial DCs, reduced dSEARCH behaviors, and lower stromal macrophage cell area. As subsets of DCs regulate the induction of various T cell subtypes that suppress allergic responses (46), our findings suggest a relative reduction in homeostatic anti-inflammatory corneal tissue responses in ocular allergy. A relative normalization of T cell dynamics was evident in individuals treated with corticosteroids or allergen-specific immunotherapy for seasonal allergy. Glucocorticoids modulate peripheral immune responses by inhibiting T cell immunity (47), while immunotherapy restores a state of natural tolerance to an allergen that is similar to non-allergic individuals (48). The quantified stabilization of T cell behavior was associated with low ocular symptoms, highlighting the potential utility of Fun-IVCM immune cell dynamics as biomarkers of therapeutic response.

Modeling acute ocular surface inflammation, 3 h of CL wear led to reduced dSEARCH activity in individual epithelial DCs (i.e., the same cells imaged pre- and post-CL wear). T cell numbers were halved in the paracentral corneal epithelium, with remaining cells showing an ~30% increase in motility. The rapid decline in

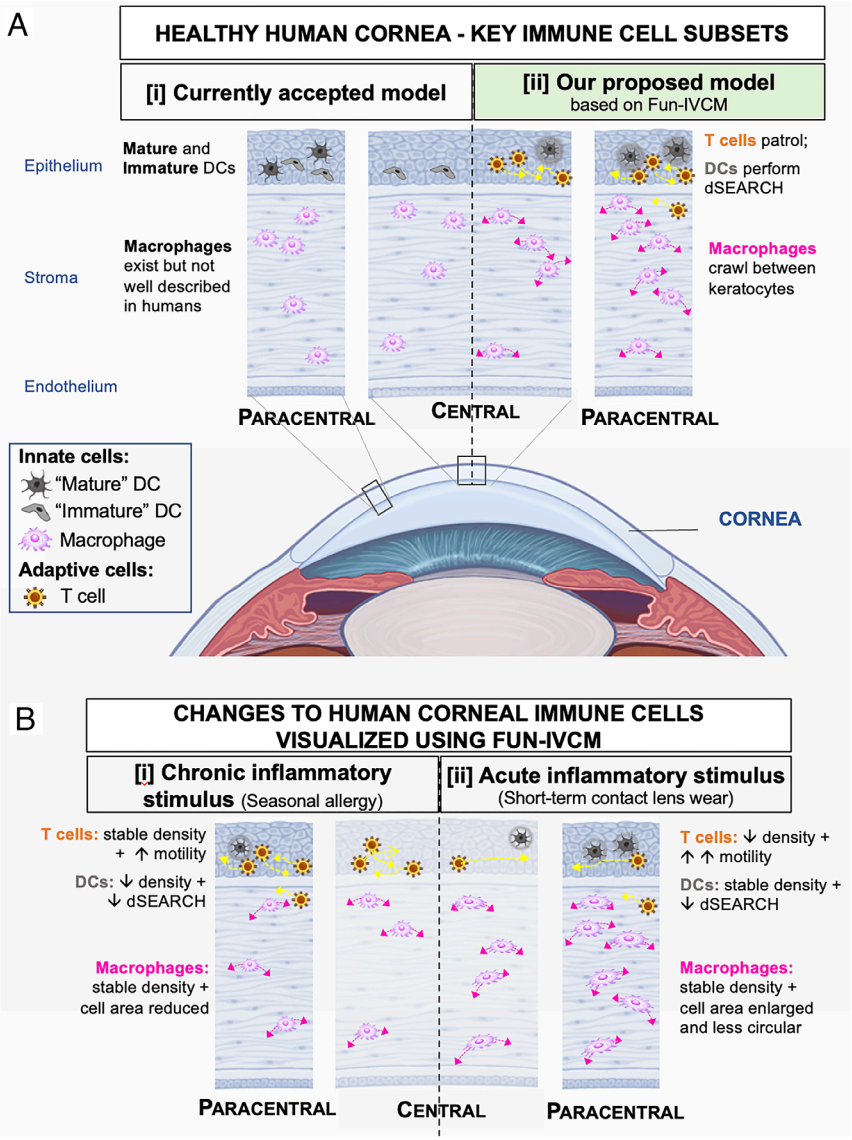

Fig. 7. (*A*) [*i*] The currently accepted model of the principle immune cell subsets in the healthy human cornea, involving "mature" and "immature" DCs in the epithelium (as imaged using traditional static IVCM) and macrophages in the stroma. [*ii*] Based on our Fun-IVCM data, we posit a role for adaptive immune cells (T cells) in homeostatic human corneal immune surveillance. Using Fun-IVCM, we identify motile T cells that patrol the epithelium and DCs that show cyclic dSEARCH behaviors; these immune cell subsets interact with each other (cell-to-cell interaction) and with sensory nerves (neuroimmune interaction). In the corneal stroma, macrophages were observed to crawl between keratocytes and to use membrane extensions consistent with the lamellipodia and/or filopodia of macrophages in other tissues. (*B*) Fun-IVCM enables insight into the in vivo effects of [*i*] chronic and [*ii*] acute inflammation on the distribution, morphology, and dynamic behaviors of corneal immune cell subsets. [*i*] In humans with symptomatic untreated seasonal allergy, T cell motility was enhanced, DC numbers were reduced, and the DCs that were present showed reduced tissue surveillance. Macrophages showed reduced cell areas. [*ii*] In response to an acute proinflammatory ocular surface stimulus (CL wear), epithelial T cells enhanced their motility and are reduced in density in the paracentral cornea; DCs show reduced dSEARCH. Stromal macrophages changed their morphological conformation, with an increased number of cellular protrusions, larger cell area, and reduction in circularity. Note: Diagrams are not to scale.

cell density may reflect either migration toward the corneal periphery and/or cell movement from the epithelium to the stroma. The potential for immune cells to traffic through the epithelial basement membrane via nerve branch points has been described for "round-shaped DCs" in the mouse cornea (10). In addition, in the underlying stroma, macrophages showed plasticity in cell shape, characterized by the appearance of additional cellular protrusions. Changes to cell shape can reflect altered cell function (49), mediated by interactions between the extracellular matrix and cell surface adhesion proteins, and changes to intracellular contractility (50). Consistent with their essential role in innate immunity, including host defense and wound healing, macrophage behavior is primarily regulated by soluble factors in their microenvironment (51). Exposing the ocular surface to a CL provoked a robust local tissue immune response that was not limited to the (outer) epithelium but also affected the stroma, suggesting active communication mechanisms across tissue layers. The differential responses of stromal macrophages with acute (i.e., CL wear) and chronic (i.e., allergy) inflammatory stimuli were interesting, with macrophages appearing smaller in corneas of allergy participants but showing an increase in cell size and lower circularity following a few hours of CL wear. Macrophage morphology (i.e., cell area and perimeter) can be an indicator of the cell activation state and phenotype. Recent immunohistochemical evidence from tumor biopsies suggests that larger tumor-associated macrophages in colorectal liver metastasis patients are prognostic of lower 5-y survival (52). How the observed differences in macrophage morphology in acute vs. chronic inflammatory scenarios in this present study relate to

macrophage activation is unclear but supports a role for Fun-IVCM for defining the in vivo inflammatory status of the human cornea.

This study demonstrates in vivo, label-free longitudinal evaluation of immune cell shape (morphological tracking) and movement (temporal tracking) through human corneal tissue (depth tracking). These data represent dynamic behaviors of immune cell subsets in the human cornea and inducible tissue-resident immune cell activation in response to a stimulus. Our data establish the utility of Fun-IVCM as a tool to identify concurrent alterations to the static and dynamic features of T cells, DCs, and macrophages, across the depth of the tissue. By adopting commercially available imaging technology, Fun-IVCM has the capacity for rapid implementation in clinical and research settings. Using the corneal whorl as a stable anatomical landmark provides a means to perform repeated imaging of the same tissue area, which facilitates time-lapsed imaging and longitudinal monitoring of cell subsets within individuals. This approach will improve the quality and consistency of immune cell analysis in clinical studies involving IVCM, which have historically been subject to sampling bias and poor repeatability. Potential applications of Fun-IVCM include developing novel biomarkers of immune cell dynamics, gleaning insight into disease pathophysiology, and evaluating the mechanistic efficacy of immune-active therapeutics.

Materials and Methods

Human Participants. Ethical approval was obtained from the University of Melbourne Human Research Ethics Committee (HREC) (ID #22828). All participants provided written informed consent to participate. Study procedures were performed in the Department of Optometry and Vision Sciences, University of Melbourne, Australia.

Participants (n = 30) were recruited from advertisements (n = 16 healthy controls) and a notification to register interest in the Melbourne Pollen App, https://www.melbournepollen.com.au/mobile-app/, (n = 14 seasonal allergy). An observational cross-sectional analysis compared healthy controls to adults experiencing mild to moderate seasonal ocular allergy symptoms (53) without concomitant medical management (n = 10, untreated allergy) to adults with seasonal allergy who recently had immunomodulatory therapy (n = 4, treated allergy). Participants attended in November or December 2021, aligning with the peak of the grass pollen season in Melbourne, Australia (54). Participant eligibility information is provided in *SI Appendix*.

IVCM Imaging. Participants' right corneas were imaged using laser-scanning IVCM, with the Heidelberg Retina Tomograph 3 and Rostock Corneal Module (Heidelberg Engineering GMB, Germany, Fig. 1*A*). Images were captured over a restricted time interval, between 09.30 AM and 02.30 PM. Prior to imaging, the ocular surface was anesthetized (Oxybuprocaine hydrochloride 0.4%, Bausch & Lomb, USA). Volume (z-stack) scans [400(x) × 400(y) × 100(z) µm], spanning the basal epithelium to mid-stroma (Fig. 1*B*), were captured at the inferonasal paracentral cornea (corneal whorl). Images were acquired as per our previous protocols (*SI Appendix*).

Fun-IVCM Video Curation and Analyses. Building on earlier proof-of-concept based on single-plane epithelial scans (55), time-lapsed IVCM videos were created in ImageJ by generating stacks that combined five to six time-separated, unique images of the same corneal region, at a consistent tissue depth (Fig. 1*C*). For analyses of the basal corneal epithelium, nerve axons were used as static features to register the image set using the TrakEM2 plugin. The image for each time point represents a single image, captured at a single focal plane. The same procedure was followed for the stroma, using stationary keratocyte nuclei as landmarks, with the exception that the image for each time point often comprised a flattened z-stack projection of two adjacent images from the raw IVCM volume scan (separated by ~2 µm, in the z-direction).

Image analyses were performed by researchers masked to participants' health status. A suite of parameters was used to define the morphology and dynamic behaviors of the immune cell subsets (*SI Appendix*, Table S3). Cell densities were calculated "per participant," for the central and paracentral cornea. All other analyses were performed at the "per cell" level (56).

Static two-dimensional (2D) immune cell morphological parameters were calculated as previously described (*SI Appendix*, Table S3) (56–58). The analysis involved using the Polygon Selections feature tool in ImageJ, to manually connect points to delineate the outermost aspects of the dendrites of individual immune cells, followed by using the Analyze–Measure function to quantify cell field area. The cell borders were then separately traced using the "freehand trace" function to quantify cell perimeter, circularity, roundness, and solidity. For DCs, the number of dendritic tips per cell was counted as a measure of dendritic complexity.

To analyze immune cell dynamics, cell motility (for T cells) and dendrite probing behavior [for DCs, (19)] data were derived in a stepwise manner using consecutive frames in the time-lapsed Fun-IVCM video (detailed in *SI Appendix*) (19).

Human Donor Tissues for Immunohistochemistry. The project was approved by the University of Melbourne HREC (ID #24637). Healthy adult human corneal tissue was obtained from a deceased donor who donated their tissue for research use, from the CERA Biobank, Centre for Eye Research Australia, Royal Victorian Eye and Ear Hospital, University of Melbourne, via the Lions Eye Donation Service. Corneas were removed at 16 h postmortem, and the tissue was stored in organ culture media for 16 d prior to fixation in 4% paraformaldehyde for 24 h and then transferred into phosphate-buffered saline (PBS) until further processing. Corneal flatmounts were immunostained to label $CD45^+$ and $CD3^+$ cells (*SI Appendix*).

Human Donor Tissues for Flow Cytometry. This study was approved by the Western Sydney Local Area Health District HREC (ID: 5080, HREC/17/WMEAD/118). Healthy human corneal tissue was obtained from deceased donors who donated their tissue for research use. Tissue was obtained within 24 h postmortem, allocated by NSW Tissue Banks, Sydney, Australia, and stored in organ culture media (MEM, Glutamax, FBS, Pen G, Step Sulfate, Amphotericin B) until collection. Corneal tissues were digested and processed for multicolor flow cytometry (*SI Appendix*).

Mice. C57BL/6, gBT-I (59), C57BL/6-Tg(UBC-GFP)30Scha/J (uGFP), C57BL/6.PL-Thy1a/CyJ (Thy1.1), gBT-I.uGFP, gBT-I.Thy1.1 mice were bred and maintained at the Peter Doherty Institute (Melbourne, Australia). B6.Cg-Tg(Itgax-Venus)1Mnz/J (CD11c-EYFP) and B6.129P2(Cg)-Cx3cr1tm1Litt/J ($CX_3CR1^{GFP/+}$) mice were bred and maintained at the Florey Institute of Neuroscience and Mental Health (FINMH, Melbourne, Australia). All experimental procedures were approved by the FINMH Animal Ethics Committee (18-093-UM) and University of Melbourne Animal Ethics Committee. For infection of mice to generate corneal memory T cells, HSV-1 KOS strain was used. Mice were adoptively transferred with 5×10^4 gBT-I $CD8^+$ T cells prior to infection. Mice were anesthetized with ketamine/xylazine (100/15 mg/kg) for infection. One drop of topical anesthetic (Alcaine 0.5%, Alcon, USA) was placed onto each eye for 5 min and then wicked off using a cotton swab. Corneas were then lightly scratched using a 30G needle; 10 µL of PBS, containing 10^6 pfu of HSV, was placed onto the eye.

Mouse Corneal Imaging. To demonstrate the dynamic behaviors of distinct cell subsets, time-lapsed movies of corneal epithelial DCs and stromal macrophages were created using explant tissue preparations from CD11c-EYFP and $CX3CR1^{GFP/+}$ mice, respectively. Excised corneas were transported to a live-cell open perfusion chamber (Round coverslip chamber; Cat #RC-25F; Harvard Apparatus, MA, USA) with a vacuum grease-sealed coverslip and 500 µL of DMEM F-12. Tissues were imaged in a temperature-controlled chamber (37 °C; 5% CO2 air flow), and confocal Z-stacks (×20 objective) were acquired every 2 min over 30 min (Leica SP8 Laser Scanning Confocal Microscope). For calculation of static cell morphometry parameters of epithelial CD11c-EYFP+ DCs and stromal $CX3CR1^{GFP/+}$ macrophages (n = 50 cells from n = 5 mice), intravital microscopy was performed using a laser confocal endoscope (FIVE2 ViewnVivo; Optiscan Imaging Ltd).

Morphometry of corneal memory gBT-I $CD8^+$ T cells (n = 30 cells from n = 9 mice) was analyzed using intravital multiphoton microscopy movies. Intravital corneal imaging was performed as previously described (18) and in *SI Appendix*.

Ex vivo mouse IVCM imaging and immunostaining were performed in CX3CR1-deficient mice containing GFP+ T cells 30 d after HSV infection (*SI Appendix*).

Statistical Analyses. Statistical analyses were performed in GraphPad Prism (version 9.0, GraphPad Software Inc., California, USA). Intergroup comparisons (healthy controls vs. untreated allergy vs. treated allergy participants) were

performed using a one-way ANOVA, following confirmation of normally distributed data using Bartlett's test. Post hoc tests involved Tukey's multiple comparisons test. Unsupervised clustering analysis was performed using PhenoGraph to identify clusters from normalized data pooled from human and mouse corneas. Principal component analysis (pca) was used to analyze the clustered human and mouse imaging cell data. Data are presented as mean ± SD, unless otherwise indicated. Correlations were examined using simple linear regression. For pre-CL vs. post-CL comparisons, unpaired *t* tests (for unmatched cells) and paired *t* tests (for matched cells) were performed. An alpha of 0.05 defined statistical significance.

Data, Materials, and Software Availability. Anonymized data for this study may become available upon request from the corresponding author, subject to approval of an ethics amendment to permit data sharing from the relevant Human Research Ethics Committee.

ACKNOWLEDGMENTS. From the University of Melbourne, we thank Ching Yi Wu for the CD3 immunostaining (Fig. 5), Haihan Jiao for assisting with the CX3CR1-eGFP time-lapsed studies, and Rajni Rajan who contributed to image analyses. We acknowledge the Florey Microscopy Facility, The Florey Institute of Neuroscience and Mental Health, for instrumentation, training, and general support. Flow cytometry was performed at the Westmead Scientific Platforms, supported by the Westmead Research Hub, Westmead Institute for Medical Research, Cancer Institute New South Wales, National Health and Medical Research Council, and the Ian Potter Foundation. We acknowledge the Lions Eye Donation Service–Centre for Eye Research Australia Biobank, Centre for Eye Research Australia, Royal Victorian Eye and Ear Hospital, University of Melbourne.

Author affiliations: [a]Department of Optometry and Vision Sciences, The University of Melbourne, Carlton, VIC 3053, Australia; [b]Department of Microbiology and Immunology, The University of Melbourne, The Peter Doherty Institute for Infection and Immunity, Melbourne, VIC 3010, Australia; [c]The Westmead Institute for Medical Research, The University of Sydney, Sydney, NSW 2145, Australia; [d]School of Optometry and Vision Science, University of New South Wales, Kensington, NSW 2052, Australia; and [e]Institute of Ophthalmology, University College London, London EC1V 9EL, United Kingdom

Author contributions: L.E.D., J.K.L., K.S., K.B., A.L.C., N.C., S.N.M., and H.R.C. designed research; L.E.D., X.Z., M.W., S.K., J.K.L., K.S., S.A., K.B., A.L.C., N.C., S.N.M., and H.R.C. performed research; L.E.D., S.N.M., and H.R.C. contributed new reagents/analytic tools; L.E.D., X.Z., M.W., S.K., S.A., K.B., A.L.C., N.C., S.N.M., and H.R.C. analyzed data; L.E.D. supervised team; L.E.D., S.N.M., and H.R.C. supervision; and L.E.D., X.Z., M.W., S.K., J.K.L., K.S., S.A., K.B., A.L.C., N.C., S.N.M., and H.R.C. wrote the paper.

1. H. R. Chinnery, X. Y. Zhang, C. Y. Wu, L. E. Downie, Corneal immune cell morphometry as an indicator of local and systemic pathology: A review. *Clin. Exp. Ophthalmol.* **49**, 729–740 (2021).
2. P. Hamrah, Q. Zhang, Y. Liu, M. R. Dana, Novel characterization of MHC class II-negative population of resident corneal Langerhans cell-type dendritic cells. *Invest. Ophthalmol. Vis. Sci.* **43**, 639–646 (2002).
3. P. Hamrah, S. O. Huq, Y. Liu, Q. Zhang, M. R. Dana, Corneal immunity is mediated by heterogeneous population of antigen-presenting cells. *J. Leukoc. Biol.* **74**, 172–178 (2003).
4. P. Hamrah, Y. Liu, Q. Zhang, M. R. Dana, The corneal stroma is endowed with a significant number of resident dendritic cells. *Invest. Ophthalmol. Vis. Sci.* **44**, 581–589 (2003).
5. H. Jiao *et al.*, Topographical and morphological differences of corneal dendritic cells during steady state and inflammation. *Ocul. Immunol. Inflamm.* **28**, 898–907 (2020).
6. J. E. Knickelbein, S. C. Watkins, P. G. McMenamin, R. L. Hendricks, Stratification of antigen-presenting cells within the normal cornea. *Ophthalmol. Eye Dis.* **1**, 45–54 (2009).
7. J. Plsková *et al.*, The immune response to corneal allograft requires a site-specific draining lymph node. *Transplantation* **73**, 210–215 (2002).
8. C. S. Brissette-Storkus, S. M. Reynolds, A. J. Lepisto, R. L. Hendricks, Identification of a novel macrophage population in the normal mouse corneal stroma. *Invest. Ophthalmol. Vis. Sci.* **43**, 2264–2271 (2002).
9. H. R. Chinnery, P. G. McMenamin, S. J. Dando, Macrophage physiology in the eye. *Pflugers Arch.* **469**, 501–515 (2017).
10. N. Gao, P. Lee, F. S. Yu, Intraepithelial dendritic cells and sensory nerves are structurally associated and functional interdependent in the cornea. *Sci. Rep.* **6**, 36414 (2016).
11. O. Stachs, R. F. Guthoff, S. Aumann, "In vivo confocal scanning laser microscopy" in *High Resolution Imaging in Microscopy and Ophthalmology: New Frontiers in Biomedical Optics [Internet]*, J. F. Bille, Ed. (Springer, Cham (CH), 2019), chap. 12.
12. J. V. Jester, P. M. Andrews, W. M. Petroll, M. A. Lemp, H. D. Cavanagh, In vivo, real-time confocal imaging. *J. Electron Microsc. Tech.* **18**, 50–60 (1991).
13. R. Mobeen *et al.*, Corneal epithelial dendritic cell density in the healthy human cornea: A meta-analysis of in-vivo confocal microscopy data. *Ocul. Surf.* **17**, 753–762 (2019).
14. J. Liu, Z. Li, Resident innate immune cells in the cornea. *Front. Immunol.* **12**, 620284 (2021).
15. N. S. Lagali *et al.*, Dendritic cell maturation in the corneal epithelium with onset of type 2 diabetes is associated with tumor necrosis factor receptor superfamily member 9. *Sci. Rep.* **8**, 14248 (2018).
16. S. J. Galli, M. Tsai, A. M. Piliponsky, The development of allergic inflammation. *Nature* **454**, 445–454 (2008).
17. N. Efron, Contact lens wear is intrinsically inflammatory. *Clin. Exp. Optom.* **100**, 3–19 (2017).
18. K. J. Loi *et al.*, Corneal tissue resident memory T cells form a unique immune compartment at the ocular surface. *Cell Rep.* **39**, 110852 (2022).
19. A. Nishibu *et al.*, Behavioral responses of epidermal Langerhans cells in situ to local pathological stimuli. *J. Invest. Dermatol.* **126**, 787–796 (2006).
20. K. M. Bertram *et al.*, Identification of HIV transmitting CD11c(+) human epidermal dendritic cells. *Nat. Commun.* **10**, 2759 (2019).
21. M. Haniffa *et al.*, Differential rates of replacement of human dermal dendritic cells and macrophages during hematopoietic stem cell transplantation. *J. Exp. Med.* **206**, 371–385 (2009).
22. N. McGovern *et al.*, Human dermal $CD14^+$ cells are a transient population of monocyte-derived macrophages. *Immunity* **41**, 465–477 (2014).
23. J. W. Rhodes *et al.*, Human anogenital monocyte-derived dendritic cells and langerin+cDC2 are major HIV targeT cells. *Nat. Commun.* **12**, 2147 (2021).
24. H. R. Chinnery *et al.*, The chemokine receptor CX3CR1 mediates homing of MHC class II-positive cells to the normal mouse corneal epithelium. *Invest. Ophthalmol. Vis. Sci.* **48**, 1568–1574 (2007).
25. R. Hao *et al.*, Analysis of globular cells in corneal nerve vortex. *Front. Med.* **9**, 806689 (2022).
26. Y. Alzahrani, N. Pritchard, N. Efron, Changes in corneal Langerhans cell density during the first few hours of contact lens wear. *Cont. Lens Anterior Eye.* **39**, 307–310 (2016).
27. L. E. Downie *et al.*, Modulating contact lens discomfort with anti-inflammatory approaches: A randomized controlled trial. *Invest. Ophthalmol. Vis. Sci.* **59**, 3755–3766 (2018).
28. R. L. Niederer, C. N. McGhee, Clinical in vivo confocal microscopy of the human cornea in health and disease. *Prog. Retin. Eye Res.* **29**, 30–58 (2010).
29. B. R. Ward *et al.*, Local thermal injury elicits immediate dynamic behavioural responses by corneal Langerhans cells. *Immunology* **120**, 556–572 (2007).
30. J. L. Stow, N. D. Condon, The cell surface environment for pathogen recognition and entry. *Clin. Transl. Immunol.* **5**, e71 (2016).
31. A. W. Taylor, Ocular immune privilege and transplantation. *Front. Immunol.* **7**, 37 (2016).
32. Y. Tan *et al.*, Role of T cell recruitment and chemokine-regulated intra-graft T cell motility patterns in corneal allograft rejection. *Am. J. Transplant.* **13**, 1461–1473 (2013).
33. G. Bitirgen *et al.*, Corneal confocal microscopy identifies corneal nerve fibre loss and increased dendritic cells in patients with long COVID. *Br. J. Ophthalmol.* **106**, 1635–1641 (2022).
34. A. Cruzat *et al.*, Inflammation and the nervous system: The connection in the cornea in patients with infectious keratitis. *Invest. Ophthalmol. Vis. Sci.* **52**, 5136–5143 (2011).
35. T. Arnous *et al.*, Tissue resident memory T cells inhabit the deep human conjunctiva. *Sci. Rep.* **12**, 6077 (2022).
36. H. Veiga-Fernandes, D. Mucida, Neuro-immune interactions at barrier surfaces. *Cell* **165**, 801–811 (2016).
37. L. Frutos-Rincón, J. A. Gómez-Sánchez, A. Íñigo-Portugués, M. C. Acosta, J. Gallar, An experimental model of neuro-immune interactions in the eye: Corneal sensory nerves and resident dendritic cells. *Int. J. Mol. Sci.* **23**, 2997 (2022).
38. H. Jiao *et al.*, Novel alterations in corneal neuroimmune phenotypes in mice with central nervous system tauopathy. *J. Neuroinflammation* **17**, 136 (2020).
39. M. Wu, L. J. Hill, L. E. Downie, H. R. Chinnery, Neuroimmune crosstalk in the cornea: The role of immune cells in corneal nerve maintenance during homeostasis and inflammation. *Prog. Retin. Eye Res.* **91**, 101105 (2022), 10.1016/j.preteyeres.2022.101105, 101105.
40. N. Gao, C. Yan, P. Lee, H. Sun, F. S. Yu, Dendritic cell dysfunction and diabetic sensory neuropathy in the cornea. *J. Clin. Investig.* **126**, 1998–2011 (2016).
41. A. T. Shenoy *et al.*, Antigen presentation by lung epithelial cells directs CD4+ TRM cell function and regulates barrier immunity. *Nat. Commun.* **12**, 5834 (2021).
42. A. Gad, A. J. Vingrys, C. Y. Wong, D. C. Jackson, L. E. Downie, Tear film inflammatory cytokine upregulation in contact lens discomfort. *Ocul. Surf.* **17**, 89–97 (2019).
43. M. F. Krummel, F. Bartumeus, A. Gérard, T cell migration, search strategies and mechanisms. *Nat. Rev. Immunol.* **16**, 193–201 (2016).
44. K. G. Sundqvist, T cell motility—How is it regulated? *Front. Immunol.* **11**, 588642 (2020).
45. A. Teijeira *et al.*, T cell migration from inflamed skin to draining lymph nodes requires intralymphatic crawling supported by ICAM-1/LFA-1 interactions. *Cell Rep.* **18**, 857–865 (2017).
46. O. Akbari, D. T. Umetsu, Role of regulatory dendritic cells in allergy and asthma. *Curr. Allergy Asthma Rep.* **5**, 56–61 (2005).
47. F. Van Laethem *et al.*, Glucocorticoids attenuate T cell receptor signaling. *J. Exp. Med.* **193**, 803–814 (2001).
48. E. Wambre, Effect of allergen-specific immunotherapy on CD4+ T cells *Curr. Opin. Allergy Clin. Immunol.* **15**, 581–587 (2015).
49. J. Folkman, A. Moscona, Role of cell shape in growth control. *Nature* **273**, 345–349 (1978).
50. J. L. Tan *et al.*, Cells lying on a bed of microneedles: An approach to isolate mechanical force. *Proc. Natl. Acad. Sci. U.S.A.* **100**, 1484–1489 (2003).
51. F. Y. McWhorter, T. Wang, P. Nguyen, T. Chung, W. F. Liu, Modulation of macrophage phenotype by cell shape. *Proc. Natl. Acad. Sci. U.S.A.* **110**, 17253–17258 (2013).
52. M. Donadon *et al.*, Macrophage morphology correlates with single-cell diversity and prognosis in colorectal liver metastasis. *J. Exp. Med.* **217**, e20191847 (2020).
53. M. Alexander *et al.*, The reliability, validity, and preliminary responsiveness of the Eye Allergy Patient Impact Questionnaire (EAPIQ). *Health Qual. Life Outcomes* **3**, 67 (2005).
54. The University of Melbourne, Why is grass pollen only counted between 1 October and 31 December? Available from: https://www.melbournepollen.com.au/faqs/why-grass-pollen-only-counted-between-1-october-and-31-december/. Accessed 27 June 2022.
55. L. H. Colorado, K. Edwards, H. R. Chinnery, H. E. Bazan, In vivo immune cell dynamics in the human cornea. *Exp. Eye Res.* **199**, 108168 (2020).
56. C. Dehghani *et al.*, Morphometric changes to corneal dendritic cells in individuals with mild cognitive impairment. *Front. Neurosci.* **14**, 556137 (2020).
57. A. Kheirkhah *et al.*, Corneal epithelial immune dendritic cell alterations in subtypes of dry eye disease: A pilot in vivo confocal microscopic study. *Invest. Ophthalmol. Vis. Sci.* **56**, 7179–7185 (2015).
58. K. Senthil, H. Jiao, L. E. Downie, H. R. Chinnery, Altered corneal epithelial dendritic cell morphology and phenotype following acute exposure to hyperosmolar saline. *Invest. Ophthalmol. Vis. Sci.* **62**, 38 (2021).
59. S. N. Mueller, W. Heath, J. D. McLain, F. R. Carbone, C. M. Jones, Characterization of two TCR transgenic mouse lines specific for herpes simplex virus. *Immunol. Cell Biol.* **80**, 156–163 (2002).